Supplementary material

1 Extended analyses of descent locations

1.1 Case-to-case variability

From the collective consideration of the trajectories of all events in Sect. 3.1 of the paper, it remains unclear whether the observed distribution of hotspots emerges as a consistent pattern from multiple events, or whether there exists pronounced case-to-case variability in terms of preferential descent locations. To shed some light onto this question, similar binned histograms are constructed for individual cases. To ensure comparability between the events (different events have a strongly varying amount of trajectories; cf. Fig. S1), the binned histogram of each event is normalized to the total number of descent segments for the respective event (Fig. S3). The four events with less than 1000 trajectories are excluded from the comparison due to their small sample size (cf. Fig. S1). For some events, the descent locations are more regionally confined to the Central Alps and the Rhine Valley (Mar 2016, Jan 2017, Feb 2017, Apr 2019; Figs. S3a, e, f, i). Yet, other events feature more widespread descent locations (Nov 2016, Apr 2018; Figs. S3d, h). However, the most striking hotspots, as for example in the Rhine Valley or in the Reuss Valley, emerge consistently among the majority of cases. This provides confidence in the chosen approach to collectively analyze all cases, as major hotspots of strong descent seem to be situated at identical locations independently of the particular meteorological situation during an event. The observed differences between cases, such as a stronger descent in some regions, might be related to the limited occurrence of foehn in a part of the regions north of the Alps. Furthermore, depending on the direction of the impinging flow, certain valley orientations (e.g., southwest to northeast) might be favored over others. A more detailed investigation of the causes for the case-to-case variability is, however, beyond the focus of this paper.

1.2 Sensitivity experiments

In addition, the sensitivity of the observed spatial distribution of descent activity with respect to the chosen thresholds (see also Sect. 2) in altitude (Δz) and time (Δt) is briefly discussed (Fig. S4). The spatial distribution features little sensitivity with respect to the tested Δt (15 min, 30 min, 60 min), indicating that most of the descent happens within shorter times, an aspect which is elaborated on in more detail in Sect. 3.2 of the paper. In contrast, varying the altitudinal threshold Δz (250 m, 500 m, 1000 m) substantially affects the number of identified descent segments. This points towards the fact that descent of larger amplitude occurs more rarely. Nevertheless, as the most striking hotspots are invariant to the changes in the thresholds, the sensitivity analysis provides confidence into the chosen values (Δz = 500 m; Δt = 30 min) and the key findings deduced in the respective Sect. 3.1.

2 Supplementary figures

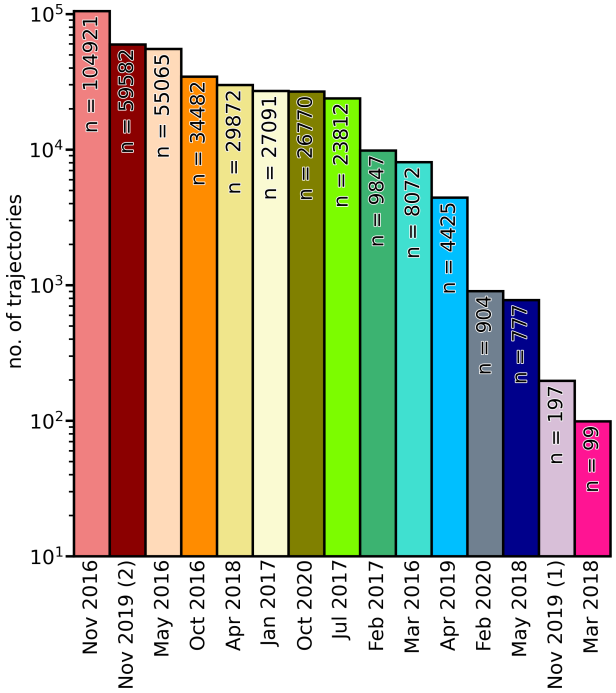

Figure S1. Total number of selected trajectories per event following the methodology as described in Sect. 2.2. Note the logarithmic y-axis.

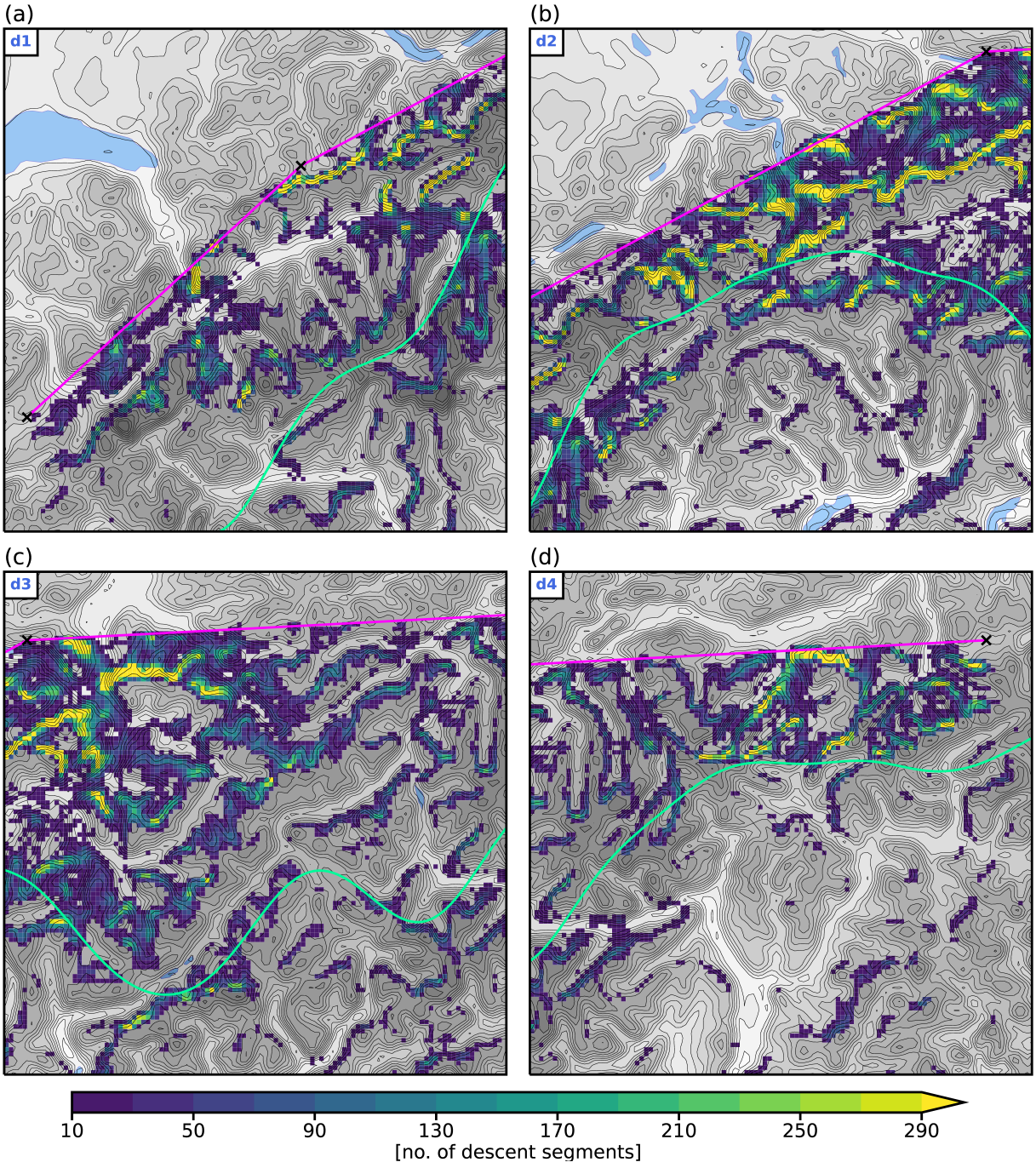

Figure S2. Same as Fig. 3 but for four subdomains (labelled d1 to d4). The subdomains are indicated by dashed blue boxes in Fig. 3.

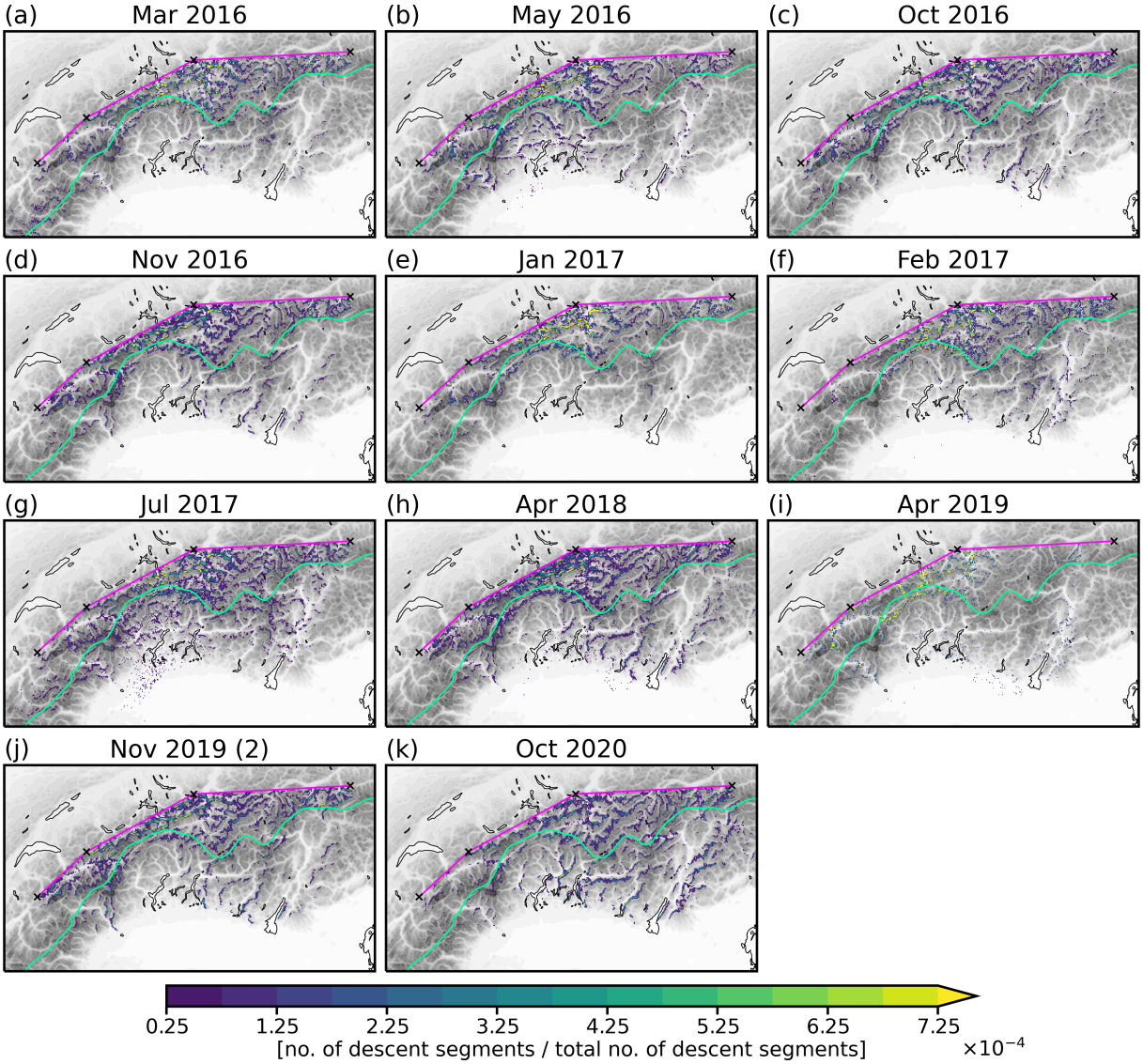

Figure S3. Same as Fig. 3 but for individual events. The number of trajectories within each bin is normalized to the total number of trajectories per event to enable a comparison between events. Note that events with less than 1000 trajectories are omitted.

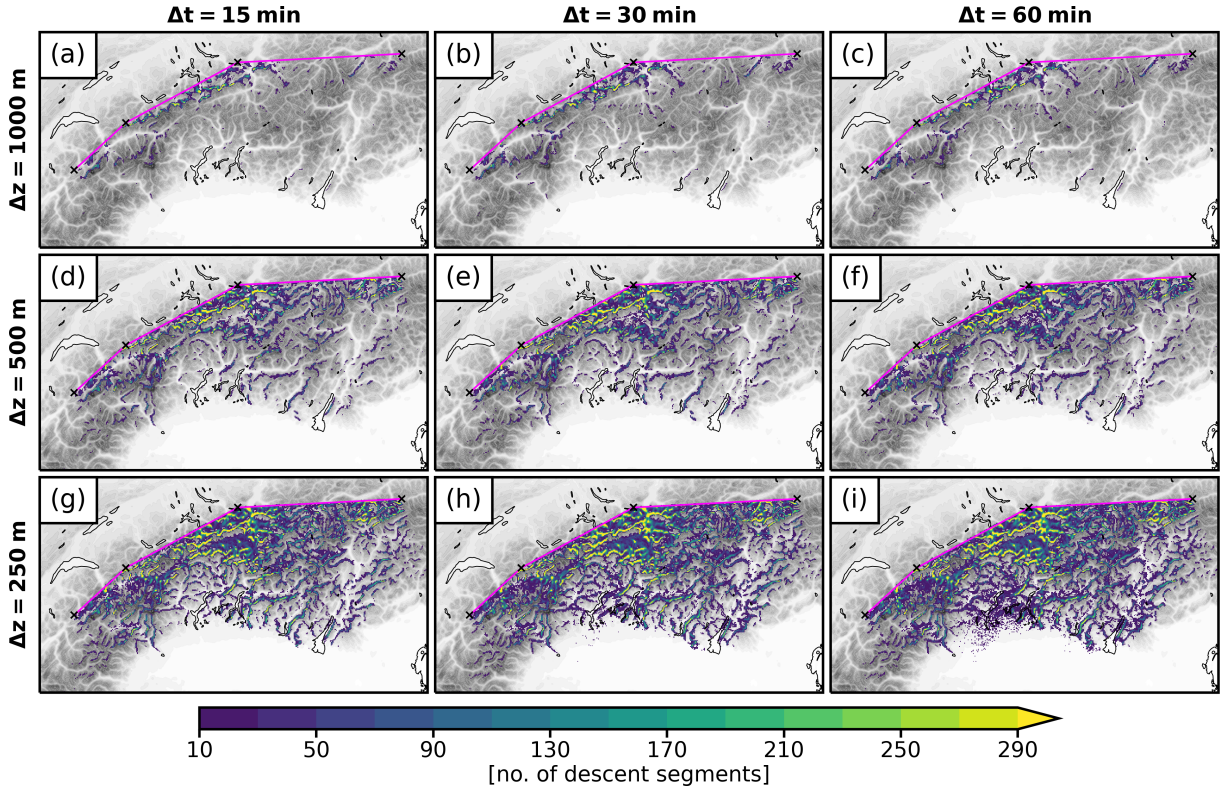

Figure S4. Same as Fig. 3, but for a set of different parameter configurations for the maximum descent duration Δt and the minimum descent magnitude Δz according to the respective row and column labels.

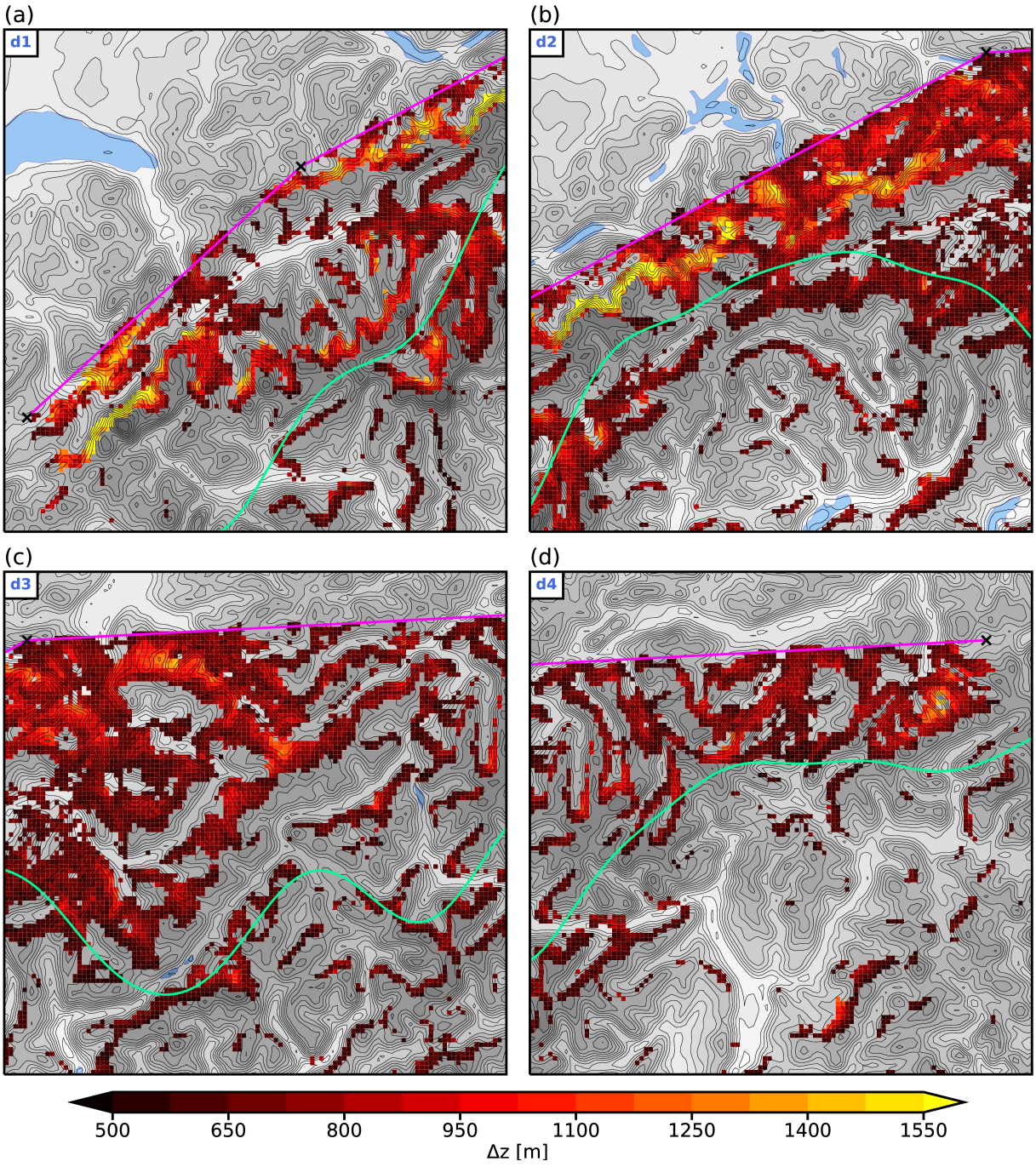

Figure S5. Same as Fig. 4b but for four subdomains (labelled d1 to d4). The subdomains are indicated by dashed blue boxes in Fig. 4b.

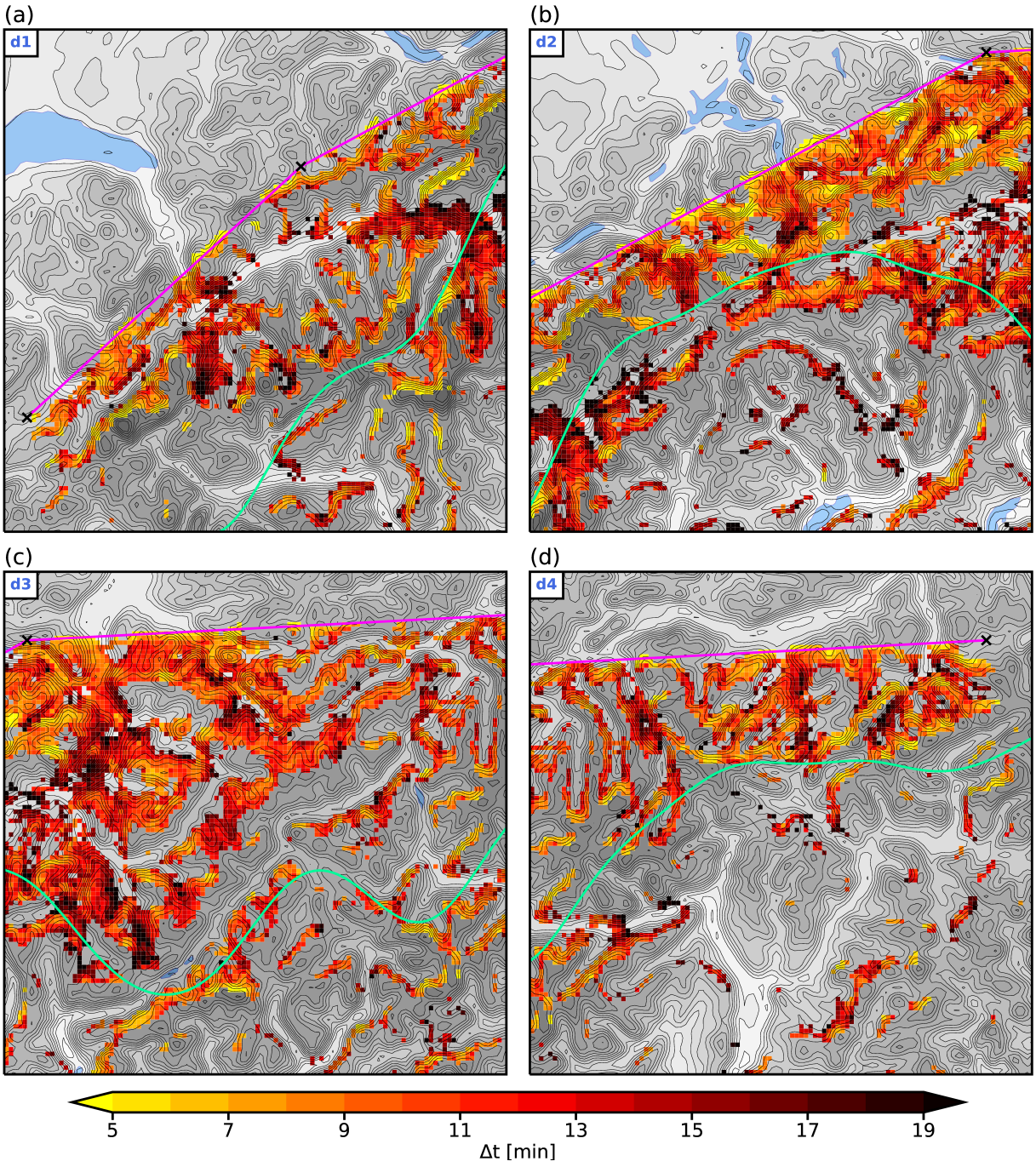

Figure S6. Same as Fig. 4d but for four subdomains (labelled d1 to d4). The subdomains are indicated by dashed blue boxes in Fig. 4b.

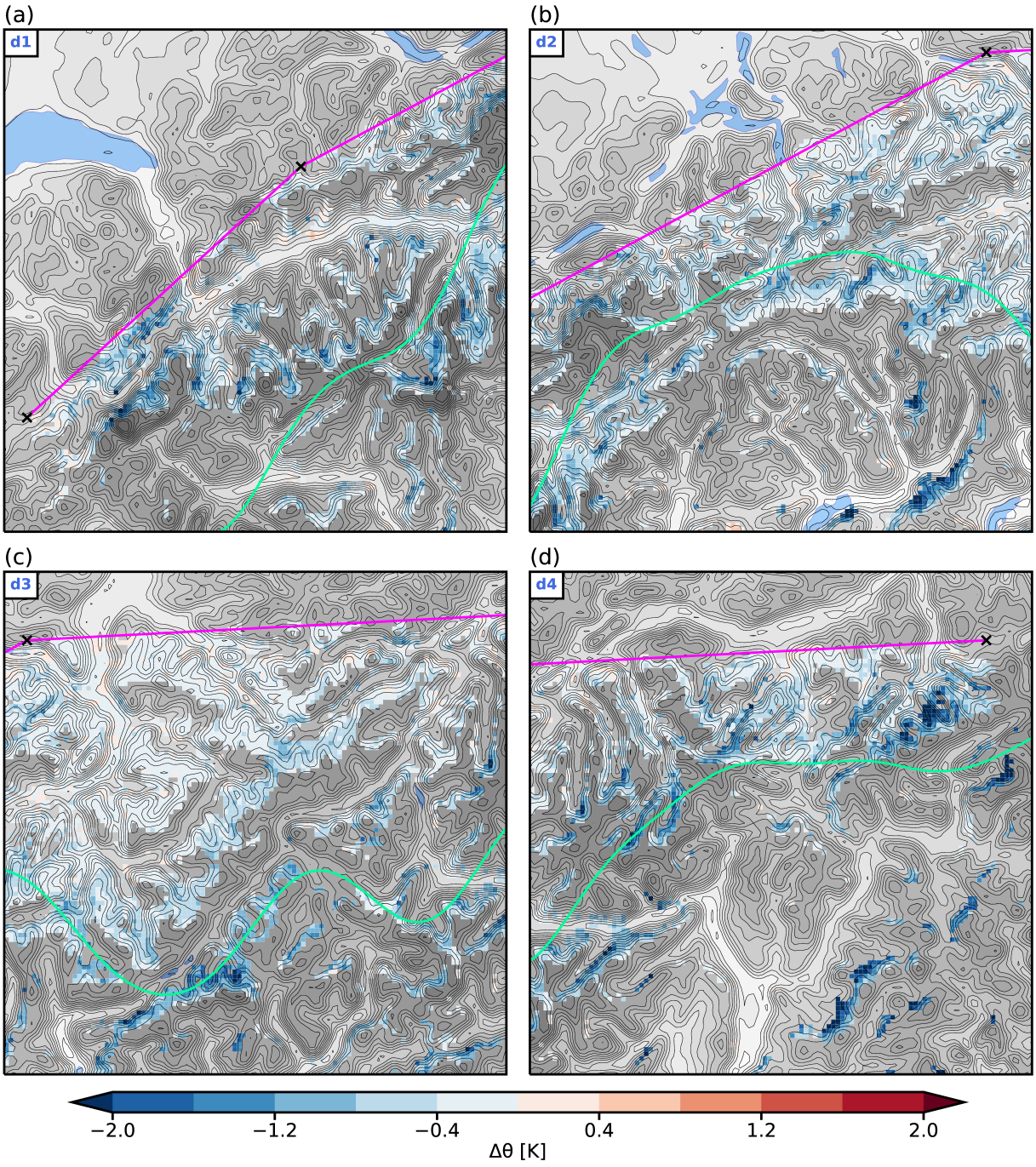

Figure S7. Same as Fig. 6b but for four subdomains (labelled d1 to d4). The subdomains are indicated by dashed blue boxes in Fig. 4b.

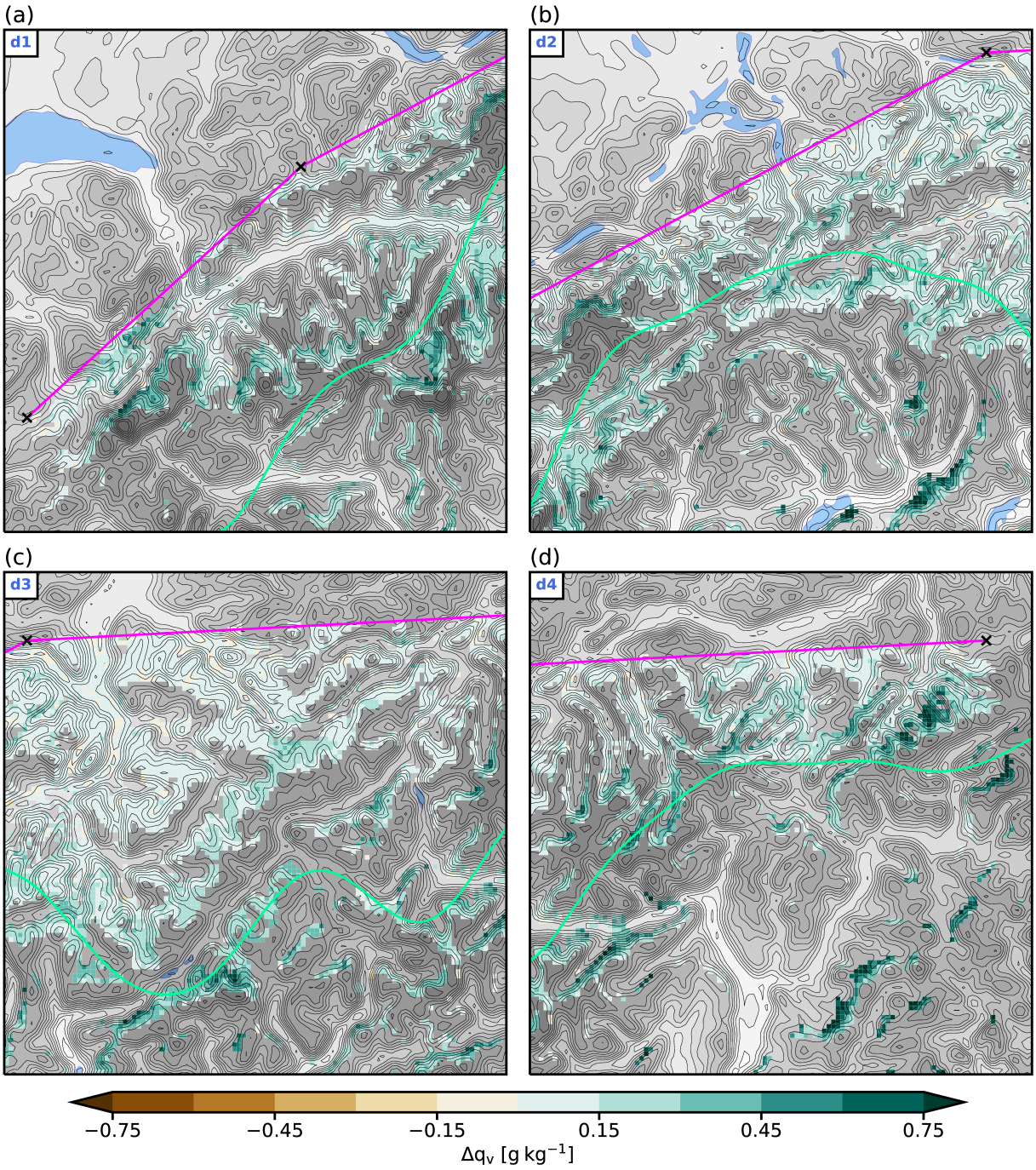

Figure S8. Same as Fig. 6d but for four subdomains (labelled d1 to d4). The subdomains are indicated by dashed blue boxes in Fig. 4b.

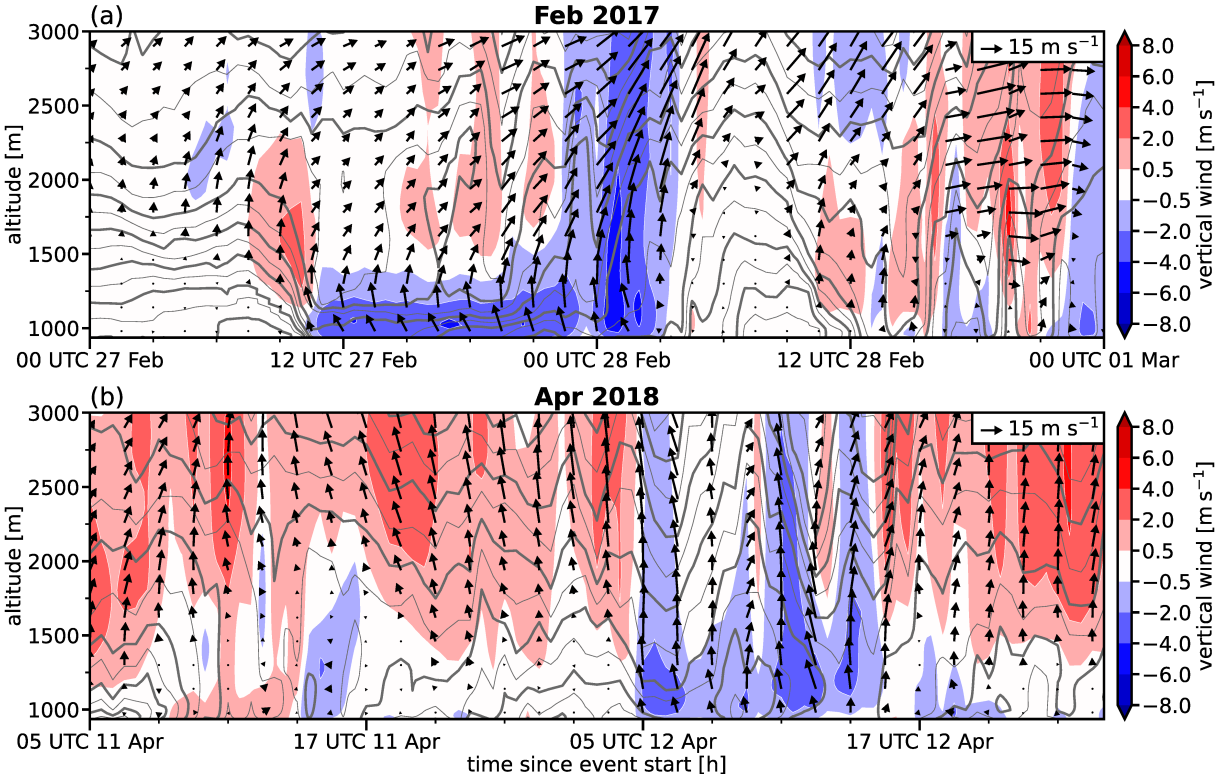

Figure S9. COSMO-based time-height diagram of vertical wind speed (colormap) and horizontal wind speed (arrows) in the concavity to the northwest of the Falknis (location of time-height diagram is indicated by dark-blue marker in Fig. 7c) for: (a) Feb 2017 event; (b) Apr 2018 event. Arrows pointing to the right correspond to eastward winds and arrows pointing upward to northward winds. Isentropes are indicated as gray contours with a spacing of 1 K.